Energy Materials

Supplementary Materials

$FeNiS_2$ quantum dot integration boosts enhanced reaction kinetics and cycle stability of SPAN nanofiber cathode for Li-S batteries

Jiajin Li[1], Ruoxi Niu[1], Haoyu Qi[1], Jinze Song[1], Yunling Wu[1,*], Lili Liu[1], Guoxing Li[1], Lijun Fu[1,*], Yuping Wu[1,2]

[1]School of Chemistry and Molecular Engineering, State Key Laboratory of Materials-Oriented Chemical Engineering, and College of Energy Science and Engineering, Nanjing Tech University, Nanjing 211816, Jiangsu, China.
[2]School of Energy and Environment, Southeast University, Nanjing 211189, Jiangsu, China.

[*]**Correspondence to:** Assoc. Prof. Yunling Wu, Prof. Lijun Fu, School of Chemistry and Molecular Engineering, State Key Laboratory of Materials-Oriented Chemical Engineering, and College of Energy Science and Engineering, Nanjing Tech University, Nanjing 211816, Jiangsu, China. E-mail: ylwu@njtech.edu.cn; l.fu@njtech.edu.cn

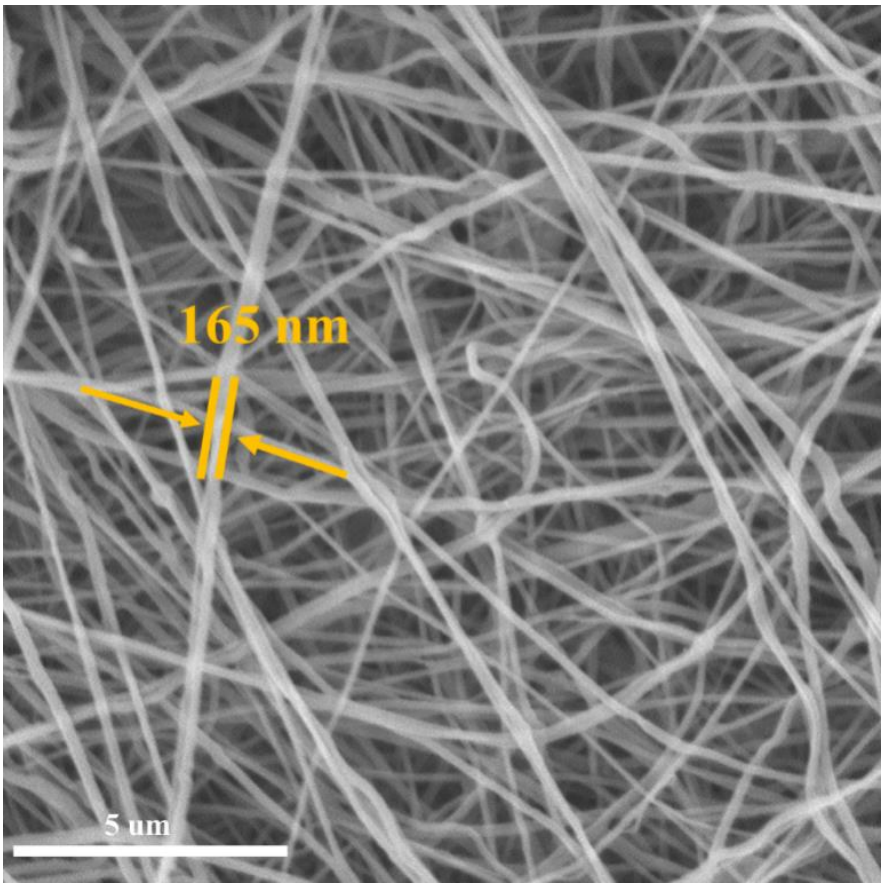

Figure S1. SEM images of $NiFe_2O_4$ QDs@PAN

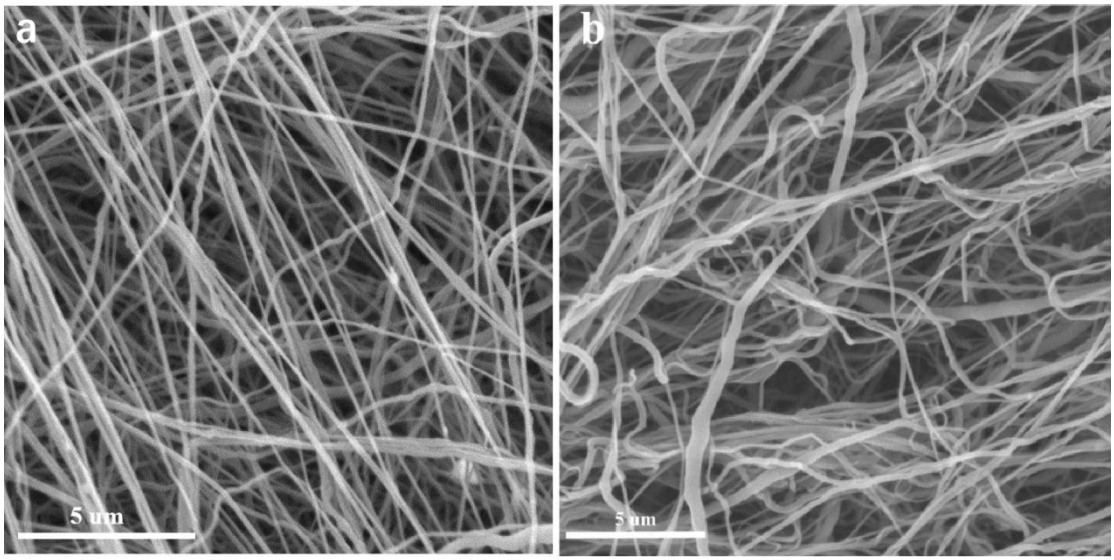

Figure S2. SEM images of (a) PAN, (b) SPAN

Table S1. Elemental analysis of SPAN

Sample	Nitrogen (wt%)	Carbon (wt%)	Hydrogen (wt%)	Sulfur (wt%)
$FeNiS_2$ QDs@SPAN	14.01	37.26	1.591	46.82
SPAN	15.82	36.69	0.494	42.1

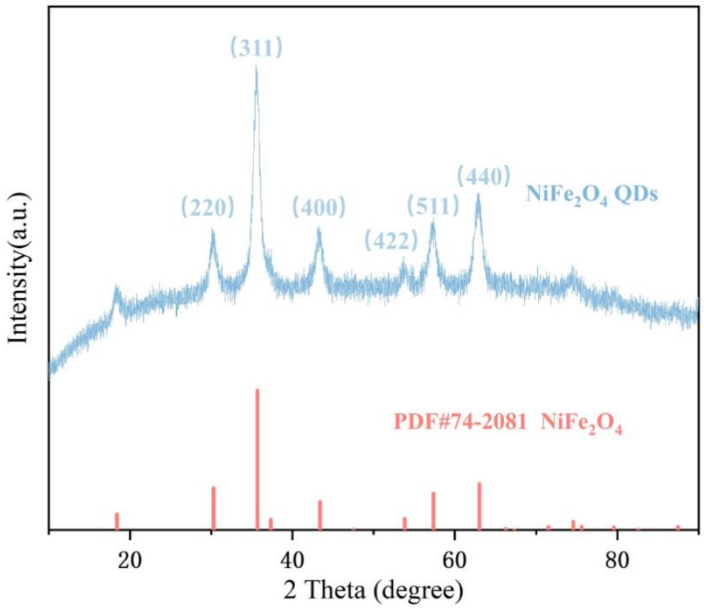

Figure S3. XRD patterns of $NiFe_2O_4$ QDs.

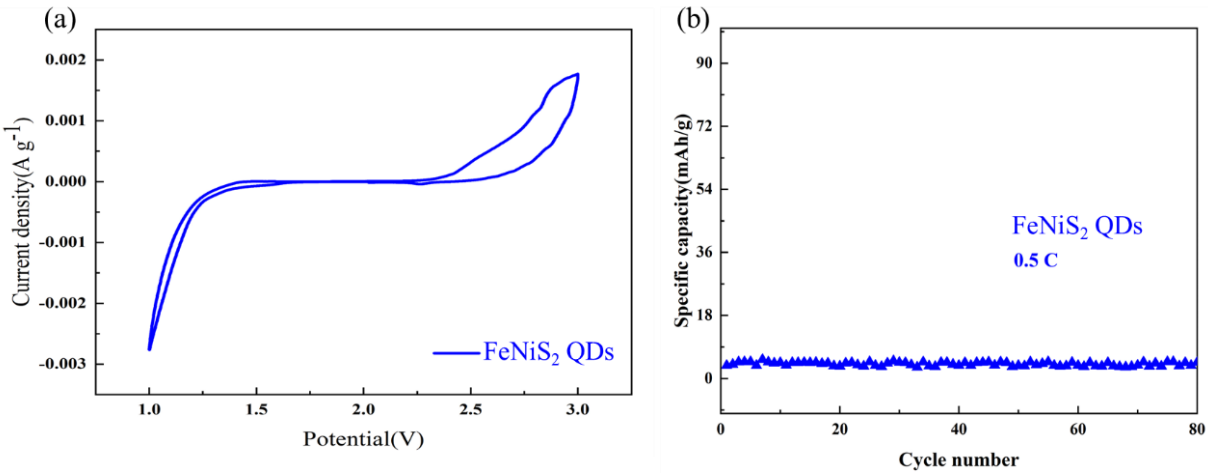

Figure S4. (a) CV curves of $FeNiS_2$ QDs; (b)Cyclic performance of the $FeNiS_2$ QDs cathode at 0.5 C.

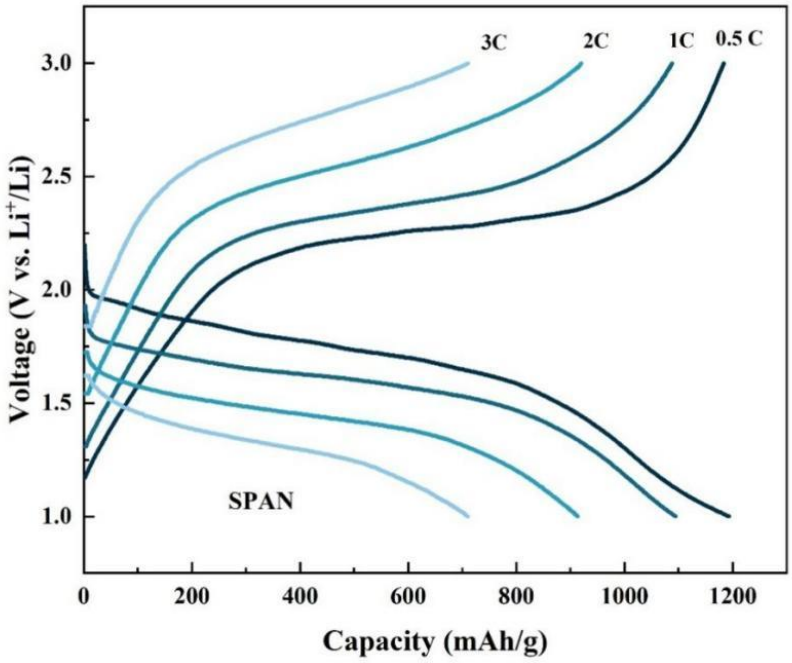

Figure S5. charge/discharge profiles of the SPAN cathode across various current rates from 0.5 to 3 C.

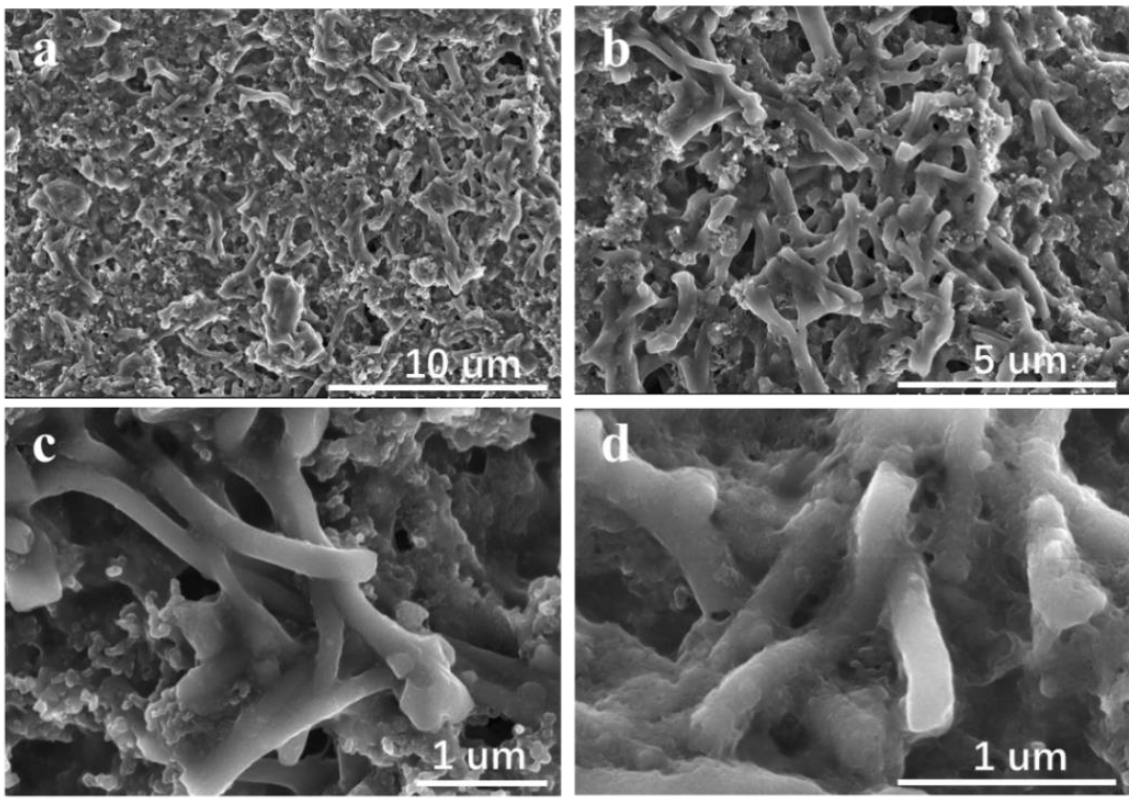

Figure S6. (a-d) SEM image of the $FeNiS_2$ QDs@SPAN cathode after 200 cycles at 1 C

Table S2. The performance comparison of this work with some similar composite. All the capacities are calculated based on the S content in the composites

	Materials [Reference]	Ratio of active materials	Areal loading (mg cm^{-2})	High C-rate, Final Cycle Capacity, Cycle No.	High-rate cycling performance (mAh g^{-1})
1	FeS_2/SPAN[1]	53.54 %	1.5-2.0	1,242 (0.335 A g^{-1}, 540 th)	N/A
2	SPAN4[3]	46 %	1.15	1000 (0.67 A g^{-1},100 th)	N/A
3	SPAN/CNT-12[4]	41.02 %	2	1180 (0.8 A g^{-1}, 800 th)	N/A
4	$Se_{0.06}$SPAN[5]	40.9 %	1-1.2	800 (0.4 A g^{-1}, 800 th)	N/A
5	SPAN@CF-RGO[6]	22.02 %	3	1200 (0.335 A g^{-1},800 th)	N/A
6	Co_{10}-SPAN-CNT[7]	41.9 %	1	1020 (1.6 A g^{-1}, 1000 th)	N/A
7	SPAN/RGO[8]	20.64 %	1-1.5	1101 (0.83 A g^{-1}, 1000 th)	N/A
8	SeS_{15}PAN[9]	55 %	1.5-2.0	1054 (0.32 A g-1, 200 th)	N/A
10	CIHP-SPAN[10]	37.74 %	2.0	800 (1.6 A g^{-1}, 1000 th)	500 (8.37 A g^{-1},500 th)
10	$FeNiS_2$ QDs@SPAN (This work)	46.82 %	1	1208 (1.6 A g^{-1}, 1000 th)	624 (8.37 A g^{-1}, 450 th)

Table S3. EIS Fitting Data for $FeNiS_2$ QDs@SPAN and SPAN Electrodes Before and After 200 Cycles at 2 C

State	$FeNiS_2$ QDs@SPAN (Rct)	SPAN (Rct)
Before cycling	124.5 Ω	198.7 Ω
After 200 cycles at 2C	18.5 Ω	38.9 Ω

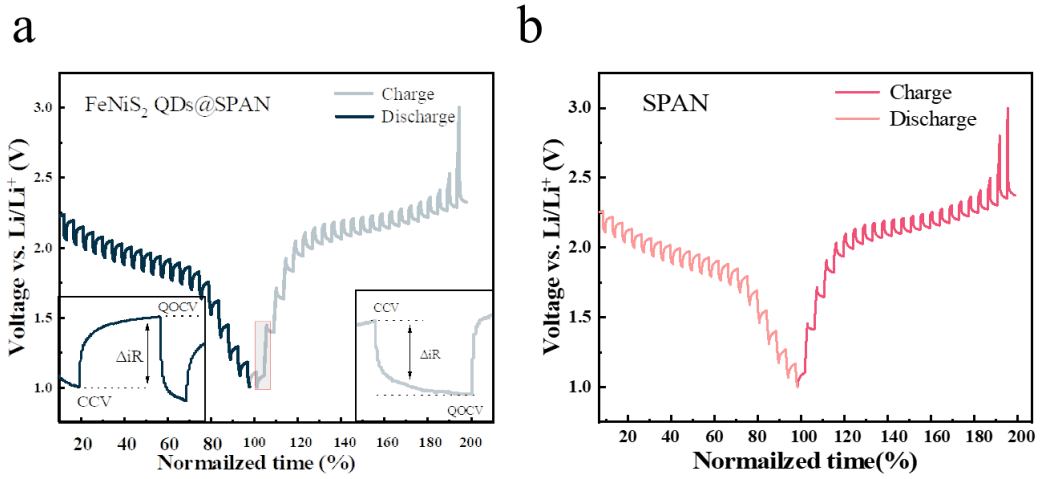

Figure S7. GITT analysis of the Li^+ diffusion kinetics. (a-b) GITT voltage profiles of the FeNiS2 QDs@SPAN and SPAN electrode at 0.1 C.

Galvanostatic intermittent titration technique (GITT) profiles were obtained at 0.1 C to further investigate the internal resistances of Li-S batteries with $FeNiS_2$ QDs@SPAN, and SPAN cathodes during discharge/charge (Figs. S7 a-b). The internal resistances for the nucleation and activation of Li_2S were illustrated by the dip depth in the charge and discharge curves (indicated by the arrows in Figs. S8a). Polarization during discharge/charge can be quantified based on the relative magnitude of $\Delta R_{internal}$ in the GITT tests, which is calculated based on equation 1.[1] The $\Delta R_{\text{internal}}$ values of the $FeNiS_2$ QDs@SPAN electrode are smaller than those of the SPAN electrode

$$\Delta R_{\text{internal}}(\Omega) = \left|\Delta V_{\text{QOCV-CCV}}\right| / I_{applied} \quad (1)$$

where $\Delta V_{\text{QOCV-CCV}}$ is the voltage difference between the quasi-open-circuit-voltage (QOCV) and closed-circuit voltage (CCV) points and $I_{applied}$ is the applied current. The $\Delta R_{\text{internal}}$ values between the Li_2S nucleation point and activation point of the $FeNiS_2$ QDs@SPAN cathode are smaller than those of the other batteries (Figs. 4f), suggesting that the $FeNiS_2$ QDs@SPAN cathode had the lowest internal resistance.

The chemical diffusion coefficient is calculated through GITT based on Fick's second law of diffusion(equation 2)[1]:

$$D_{Li+} = \frac{4}{\pi\tau}\left(\frac{n_m V_m}{S}\right)^2 \left(\frac{\Delta E_S}{\Delta E_t}\right)^2 \quad (2)$$

Where τ is the duration of the current pulse, n_m is the mole number of the electrode materials, V_m is the molar volume of the electrode materials, S is the contact area between electrode and electrolyte, ΔE_S is the change in the steady-state voltage at the end of the relaxation period over a single galvanostatic titration and ΔE_t is the total change of cell voltage during a constant-current pulse.

The findings reveal that the overall diffusion coefficient of Li^+ within the $FeNiS_2$ QDs@SPAN cathode surpasses that of the SPAN electrode (Figs. 4g). This indicates a significant enhancement in the Li^+ diffusion kinetics within the $FeNiS_2$ QDs@SPAN electrode, featuring faster charge transfer kinetics or excellent sulfur reduction kinetics.

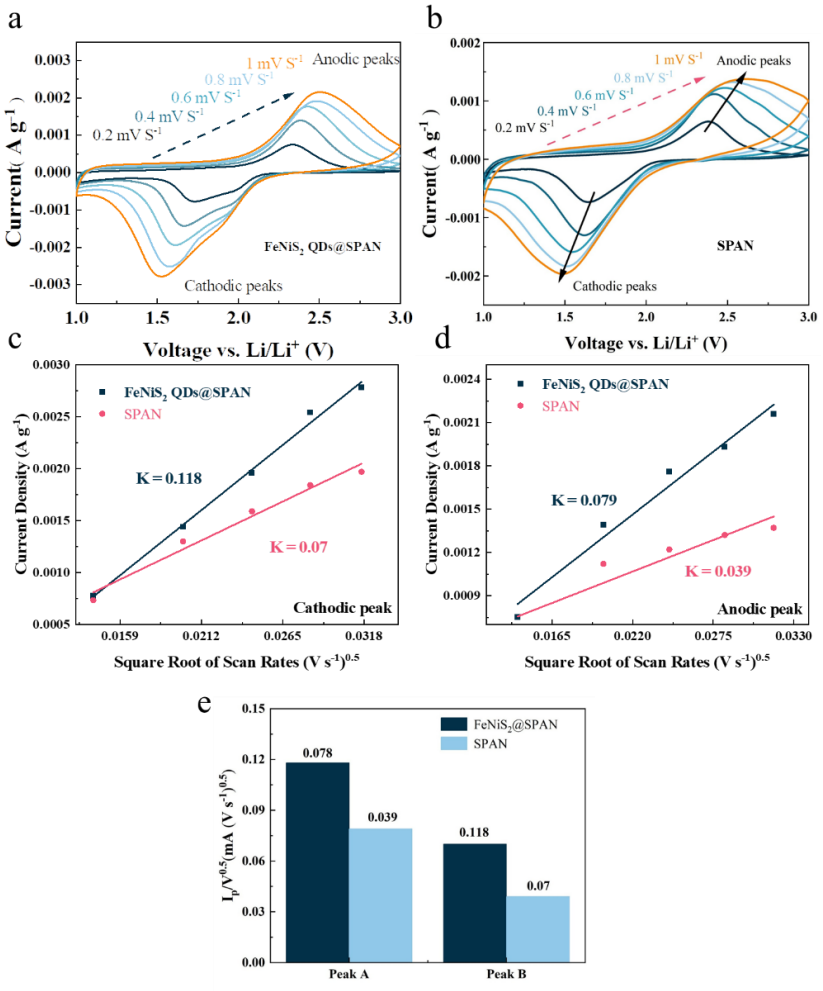

Figure S8. CV analysis of the reaction kinetics and ion diffusion behavior. (a-b) CV curves of the $FeNiS_2$ QDs@SPAN and SPAN, electrodes at various scanning rates. Plot of CV peak current of peak A, peak B (c-d) versus the square root of scan rates. (e) Plot of CV peak current of peak A and peak B versus the square root of scan rates and corresponding fitted slopes.

Under a range of scan rates from 0.2 to 1 mV s^{-1}, CV tests were conducted on both cathode materials to assess the impact of quantum dots on the electrode redox kinetics, as depicted in Figs S9 a-b. The process can be described using the Randles-Sevcik equation：[2]

$$I_p = (2.69 \times 10^5) n^{1.5} A D^{0.5} C \nu^{0.5} \quad (3)$$

where I_p represents the peak current density, n represents thenumber of charge transfers, A represents the area of electrode, D represents the Li^+ diffusion coefficient, C represents the Li^+ concentration, and ν represents the potential scanning rate. The linear relationship between the current density of the anodic and cathodic peaks and the square root of the scan rate for all electrodes indicates a diffusion-limited process. The slope of the curve (Figs. S8c-d) is directly proportional to the Li^+ diffusion, with the $FeNiS_2$ QDs@SPAN cathode showing the highest slope, suggesting the highest Li^+ diffusion rate (Figs. S8e). The high catalytic activity of $FeNiS_2$ QDs facilitates rapid diffusion of lithium ions, contributing to the enhanced conversion of Li_2S.

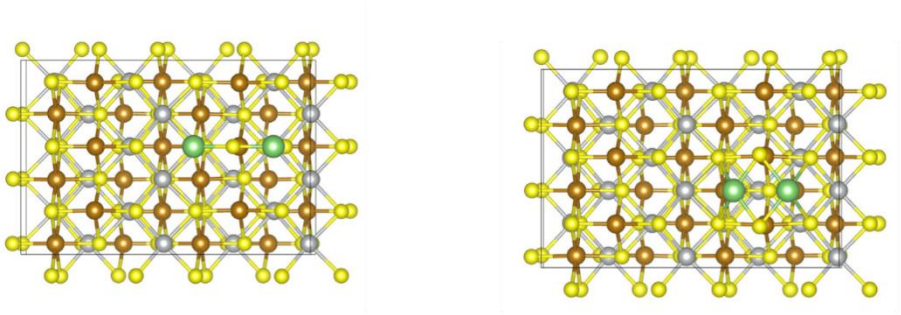

Figure S9. Top view of optimized structures of Li_2S and Li_2S_2 on $FeNiS_2$ (102) surface.

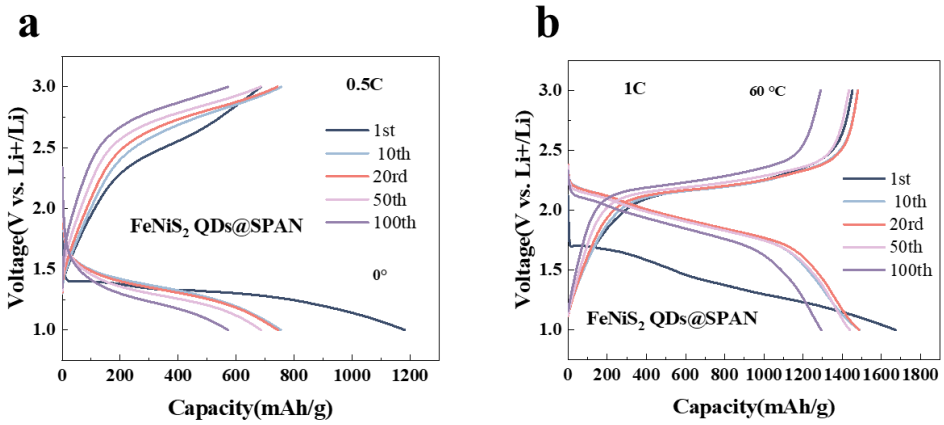

Figure S10. Galvanostatic charge-discharge profiles of $FeNiS_2$ QDs@SPAN and SPAN electrodes under varying temperature and current density conditions. (a) present the charge-discharge curves of $FeNiS_2$ QDs@SPAN and SPAN electrodes at a 0.5C rate and 0 °C. (b) present the charge-discharge curves of $FeNiS_2$ QDs@SPAN and SPAN electrodes at a 1C rate and 60 °C.

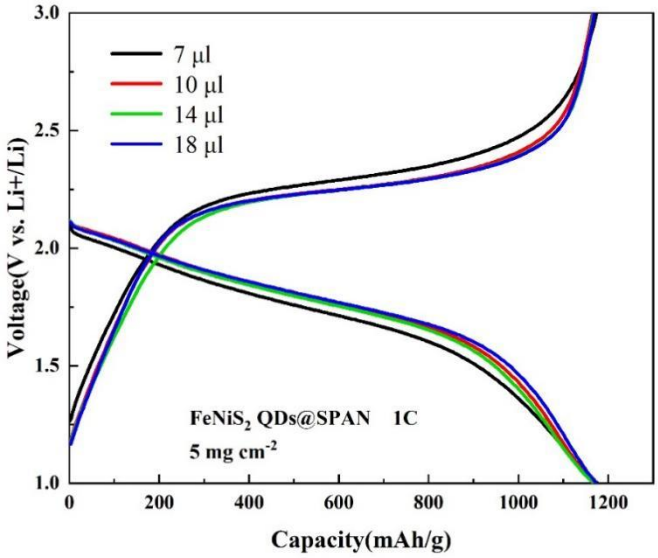

Figure S11. Charge/discharge curves of $FeNiS_2$ QDs@SPAN during the 3rd cycle at 5 mg cm^{-2} area sulfur loading with different E/S.

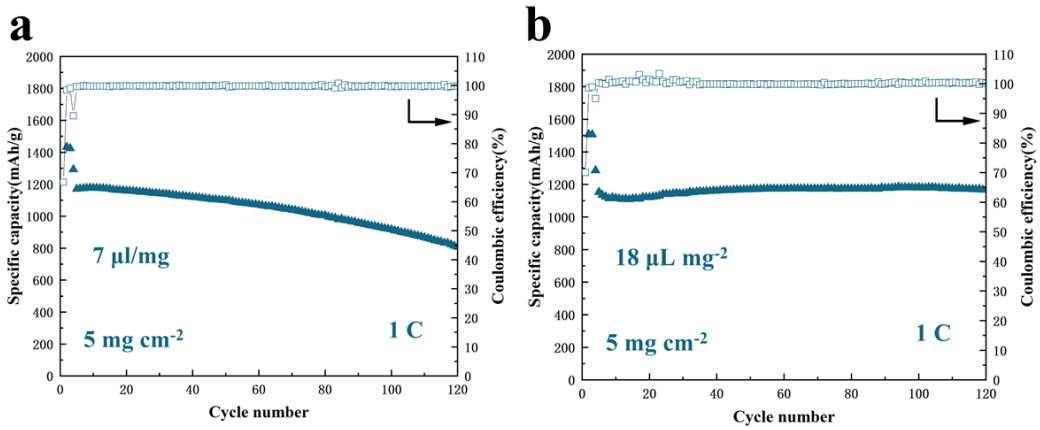

Figure S12. Evaluation of cycling stability influenced by E/S ratio. (a-b) illustrate the cycling performance of the $FeNiS_2$ QDs@SPAN electrode at various electrolyte-to-sulfur (E/S) ratios of 7 and 18 µL mg^{-1}, tested at a rate of 1 C.

REFERENCE

1. Hao, C.; Liu, J.; Wang, Q.; Wang, L.; Zhang, X.; Yang, J.; NuLi, Y.; Lu, H.; Wang, J. High Volumetric Capacity FeS_2/SPAN Composite with Promoted Kinetics for Li-S Battery. *ACS Nano*. 2025, 19, 25385-25394. https://doi.org/10.1021/acsnano.5c06966
2. Li, Y.; He, R.; Liu, H.; Zhang, Y.; Liu, H.; Han, N.; Zhang, X. Construction of CoS_2 Reduction Accelerator-Modified Sulfurized Polyacrylonitrile Nanofibers as High-Performance Cathode Materials for Practical Lithium-Sulfur Batteries. *ACS Appl. Energy Mater.* 2023, 6, 8466-8478. https://doi.org/10.1021/acsaem.3c01284
3. Liu, Y.; Wang, W.; Wang, A.; Jin, Z.; Zhao, H.; Yang, Y. A polysulfide reduction accelerator -NiS_2-modified sulfurized polyacrylonitrile as a high performance cathode material for lithium-sulfur batteries. *J. Mater. Chem. A*. 2017, 5, 22120-22124. https://doi.org/10.1039/C7TA04279E
4. Wang, X.; Qian, Y.; Wang, L.; Yang, H.; Li, H.; Zhao, Y.; Liu, T. Sulfurized Polyacrylonitrile Cathodes with High Compatibility in Both Ether and Carbonate Electrolytes for Ultrastable Lithium-Sulfur Batteries. *Adv. Funct. Mater.* 2019, 29, 1902929. https://doi.org/10.1002/adfm.201902929
5. Chen, X.; Peng, L.; Wang, L.; Yang, J.; Hao, Z.; Xiang, J.; Yuan, K.; Huang, Y.; Shan, B.; Yuan, L.; Xie, J. Ether-compatible sulfurized polyacrylonitrile cathode with excellent performance enabled by fast kinetics via selenium doping. *Nat. Commun.* 2019, 10, https://doi.org/1021. 10.1038/s41467-019-08818-6
6. Lu, J.; Zhang, Y.; Huang, J.; Jiang, H.; Liang, B.; Wang, B.; He, D.; Chen, H. Melamine foam-derived N-doped carbon framework and graphene-supported sulfurized polyacrylonitrile for high performance lithium-sulfur battery cathode. *J. Energy Storage*. 2025, 118, 116330. https://doi.org/10.1016/j.est.2025.116330
7. Abdul Razzaq, A.; Chen, G.; Zhao, X.; Yuan, X.; Hu, J.; Li, Z.; Chen, Y.; Xu, J.; Shah, R.; Zhong, J.; Peng, Y.; Deng, Z. Cobalt coordination with pyridines in sulfurized polyacrylonitrile cathodes to form conductive pathways and catalytic M-N_4S sites for accelerated Li-S kinetics. *J. Energy Chem.* 2021, 61, 170-178. https://doi.org/10.1016/j.jechem.2021.01.012
8. Lu, J.; Zhang, Y.; Huang, J.; Jiang, H.; Liang, B.; Wang, B.; He, D.; Chen, H. A free-standing sulfide polyacrylonitrile/reduced graphene oxide film cathode with nacre-like architecture for high-performance lithium-sulfur batteries. *J. Power Sources*. 2025, 629, 235916. https://doi.org/10.1016/j.jpowsour.2024.235916
9. Liu, H.; Zhang, Y.; Li, Y.; Han, N.; Liu, H.; Zhang, X. Solid-State Transformations of Active Materials in the Pores of Sulfurized-Polyacrylonitrile Fiber Membranes via Nucleophilic Reactions for High-Loading and Free-Standing Lithium-Sulfur Battery Cathodes. *Adv. Fiber Mater.* 2024, 6, 772-785. https://doi.org/10.1007/s42765-024-00391-y
10. Shao, J.; Huang, C.; Zhu, Q.; Sun, N.; Zhang, J.; Wang, R.; Chen, Y.; Zhang, Z. Flexible CNT-Interpenetrating Hierarchically Porous Sulfurized Polyacrylonitrile (CIHP-SPAN) Electrodes for High-Rate Lithium-Sulfur (Li-S) Batteries. *Nanomaterials*. 2024, 14, 1155. https://doi.org/10.3390/nano14131155